Human galectin-9 potently enhances SARS-CoV-2 replication and inflammation in airway epithelial cells

Li Du[1,2], Mohamed S. Bouzidi[1,2], Akshay Gala[1,2], Fred Deiter[3,4], Jean-Noël Billaud[5], Stephen T. Yeung[6], Prerna Dabral[1,2], Jing Jin[1,2], Graham Simmons[1,2], Zain Y. Dossani[1,2], Toshiro Niki[7], Lishomwa C. Ndhlovu[6], John R. Greenland[3,4], Satish K. Pillai[1,2,*]

[1]Vitalant Research Institute, San Francisco, CA 94105, USA.

[2]Department of Laboratory Medicine, University of California, San Francisco, CA 94143-0134, USA.

[3]Department of Medicine, University of California, San Francisco, CA 94143-0410, USA.

[4]Veterans Affairs Health Care System, San Francisco, CA 94121, USA.

[5]QIAGEN Digital Insights, Redwood City, CA 94063, USA.

[6]Division of Infectious Diseases, Department of Medicine, Weill Cornell Medicine, New York, NY 10021, USA.

[7]Kagawa University, Kagawa 760-0016, Japan.

*Correspondence to: Satish K. Pillai, E-mail: satish.pillai@ucsf.edu

Abstract

The severe acute respiratory syndrome coronavirus 2 (SARS-CoV-2) pandemic has caused a global economic and health crisis. Recently, plasma levels of galectin-9 (Gal-9), a β-galactoside-binding lectin involved in immune regulation and viral immunopathogenesis, were reported to be elevated in the setting of severe COVID-19 disease. However, the impact of Gal-9 on SARS-CoV-2 infection and immunopathology remained to be elucidated. In this study, we demonstrate that Gal-9 treatment potently enhances SARS-CoV-2 replication in human airway epithelial cells (AECs), including immortalized AECs and primary AECs cultured at the air–liquid interface. Gal-9–glycan interactions promote SARS-CoV-2 attachment and entry into AECs in an angiotensin-converting enzyme 2 (ACE2)-dependent manner, enhancing the binding of the viral spike protein to ACE2. Transcriptomic analysis revealed that Gal-9 and SARS-CoV-2 infection synergistically induced the expression of key pro-inflammatory programs in AECs including the IL-6, IL-8, IL-17, EIF2, and TNFα signaling pathways. Our findings suggest that manipulation of Gal-9 should be explored as a therapeutic strategy for SARS-CoV-2 infection.

Keywords: SARS-CoV-2, galectin-9, inflammation, airway epithelial cells

Introduction

The first known case of coronavirus disease 2019 (COVID-19), caused by severe acute respiratory syndrome coronavirus 2 (SARS-CoV-2) infection, was reported in December 2019. Rapidly, COVID-19 cases were reported worldwide. To date, SARS-CoV-2 has accounted for more than 620 million infections and more than 6.5 million deaths worldwide (Dong et al., 2020). The rapid spread of SARS-CoV-2 continues to have a major impact on global health and the economy. COVID-19 is mainly characterized by pneumonia, including fever, cough, and chest discomfort, and in severe cases dyspnea and lung infiltration (Hu et al., 2021).

The major cause of death in COVID-19 cases is acute respiratory distress syndrome (ARDS) accompanied by a cytokine storm (Hojyo et al., 2020). Several reports have identified specific circulating proteins and cytokines in blood plasma that are elevated in the setting of COVID-19 and may constitute clinically useful disease biomarkers (Del Valle et al., 2020; Han et al., 2020). One such specific protein is galectin-9 (Gal-9). Studies have recently revealed that plasma Gal-9 levels are elevated in COVID-19 patients and are positively correlated with COVID-19 severity (Bai et al., 2021; Bozorgmehr et al., 2021; Chen et al., 2021; Patel et al., 2021). Furthermore, plasma levels of Gal-9 during COVID-19 were positively correlated with key pro-inflammatory cytokines, including interleukin 6 (IL-6), interferon gamma-induced protein 10, and

tumor necrosis factor alpha (TNFα) (Bozorgmehr et al., 2021). However, the mechanism linking Gal-9 to severe COVID-19 disease remains to be elucidated.

Gal-9, encoded by the *LGALS9* gene, belongs to the galectin family, which includes 15 carbohydrate binding proteins sharing a common carbohydrate-recognition domain (CRD) (Miyanishi et al., 2007). Conserved CRDs can bind to β-galactoside containing glycans (Miyanishi et al., 2007). Many members of the galectin family, including Gal-9, are able to recognize Poly-N-acetyllactosamine (poly-LacNAc) structures occurring in both *N-* and *O-*linked glycans (Lujan et al., 2018). Gal-9 is known for its regulation of immune responses and viral pathogenesis through glycan-mediated recognition. It is ubiquitously expressed in different tissues and cells in humans (e.g. endothelial cells, T lymphocytes, dendritic cells, macrophages, intestinal epithelial cells), and is localized in the extracellular matrix, surface, cytoplasm, and nucleus of cells (Shahbaz et al., 2020). Circulating levels of Gal-9 serve as sensitive and non-invasive biomarkers in a broad range of conditions including cancer, autoimmunity, and infectious diseases, and the roles of Gal-9 vary with respect to cell type and disease state (Moar and Tandon, 2021). For example, Gal-9 suppresses antigen-specific CD8^{+} T cell effector functions via interaction with its receptor, TIM-3 (Sehrawat et al., 2010), and the Gal-9/TIM-3 axis promotes tumor survival through cross-talk with the PD-1 immune checkpoint (Yang et al., 2021). The functions of Gal-9 in the inflammatory response have been studied extensively. Gal-9 enhances cytokine secretion in the human mast cell line (Kojima et al., 2014), and potentiates secretion of pro-inflammatory cytokines in inflammatory models of arthritis via interaction with TIM-3 (Anderson et al., 2007). In specific relevance to viral pathogenesis, Gal-9 can bind to glycan structures expressed on the

surface of both host cells and microorganisms to modulate antiviral immunity, and to promote or inhibit viral infection and replication (Machala et al., 2019). Gal-9 was demonstrated to inhibit human cytomegalovirus infection by its CRDs (Machala et al., 2019). In hepatitis C virus (HCV)-infected individuals, virus infection induces Gal-9 secretion, which in turn induces pro-inflammatory cytokines leading to depletion of CD4^{+} T cells, apoptosis of HCV-specific cytotoxic T cells, and expansion of regulatory T cells (Zhuo et al., 2017). Gal-9 is elevated in human immunodeficiency virus-1 (HIV-1)-infected individuals (Abdel-Mohsen et al., 2016; Premeaux et al., 2019), mediates HIV-1 transcription and reactivation (Abdel-Mohsen et al., 2016; Sanz et al., 2021), and potentiates HIV-1 infection by regulating the T cell surface redox environment (Bi et al., 2011). These previous reports provide compelling evidence of the diverse roles of Gal-9 in viral infection and virus-associated immunopathology.

To date, a causal role of Gal-9 in SARS-CoV-2 pathology has not been demonstrated. To address this gap, we investigated the effects of Gal-9 treatment on SARS-CoV-2 replication and pro-inflammatory signaling in immortalized and primary human airway epithelial cells (AECs). Our data show that Gal-9 facilitates SARS-CoV-2 replication and promotes virus-associated immunopathology in the human airway, motivating exploration into Gal-9 manipulation as a therapeutic strategy for COVID-19 disease.

Results

Gal-9 potently enhances SARS-CoV-2 replication in Calu-3 cells

To investigate the impact of Gal-9 on SARS-CoV-2 infection, we first determined the natural expression of Gal-9 in human AECs with or without SARS-CoV-2 infection. In line with the undetected Gal-9 protein expression in alveolar epithelial cells (Lindskog, 2016), the mean Gal-9 level in culture medium or on the cell surface of Calu-3 cells and primary AECs was negligible (Supplementary Figure S1). Moreover, Gal-9 level was unaffected by SARS-CoV-2 infection (Supplementary Figure S1), implying that the elevated plasma Gal-9 level observed in COVID-19 patients is derived from other cell sources. Therefore, we used a recombinant stable-form of Gal-9 in human AECs to mimic endogenously produced Gal-9. To optimize dosing for *in vitro* experiments, we relied on previously published measurements of Gal-9 concentrations *in vivo* during COVID-19 disease, and we determined the cytotoxicity of recombinant stable-form Gal-9. Recent studies have demonstrated that the mean plasma Gal-9 concentration in COVID-19 patients was 2250 ng/ml, as compared to 450 ng/ml in healthy controls (Iwasaki-Hozumi et al., 2021), and Gal-9 expression is significantly higher in pulmonary tissues than in plasma (Matsumoto et al., 2013). The 50% cytotoxic concentration (CC_{50}) value for Gal-9 in Calu-3 cells was 597 nM (19700 ng/ml) as determined by MTT assay (Figure 1A). Based on these criteria, we chose to test the effects of Gal-9 on SARS-CoV-2 replication at 50 nM (1650 ng/ml), 100 nM (3295 ng/ml), and 250 nM (8235 ng/ml) concentrations. Calu-3 cells were pre-treated with Gal-9 for six hours before viral infection (MOI = 0.01), and Gal-9 was maintained in the media until 24 hours following infection. SARS-CoV-2 infection, as measured by quantitation of viral nucleocapsid (*N*)

gene expression, was increased significantly by treatment with Gal-9 in a dose dependent manner ($P < 0.0001$) (Figure 1B), with up to 27-fold induction at the highest concentration of Gal-9. Similarly, release of infectious virus in the supernatant was enhanced significantly by Gal-9 in a dose dependent manner, as measured by median tissue culture infectious dose ($TCID_{50}$) ($P < 0.05$) (Figure 1C). The enhancement of virus production by Gal-9 was confirmed by specific staining of viral N protein using an immunofluorescence assay (Figure 1D and E). Taken together, these data demonstrate that Gal-9 increases SARS-CoV-2 viral production in susceptible Calu-3 cells.

Gal-9 enhances SARS-CoV-2 entry in an ACE2-dependent manner

To investigate the stage of the virus replication cycle impacted by Gal-9, we treated Calu-3 cells with Gal-9 at the concentration of 250 nM, chosen based on our analyses of toxicity and dose response. Calu-3 cells were treated with Gal-9 before and after virus infection. Protocols are illustrated in Supplementary Figure S2A. Gal-9-mediated enhancement of virus production was significantly higher in pre-treated cells ($P < 0.05$), as compared to cells treated with Gal-9 following viral exposure (Supplementary Figure S2B). These results suggested that Gal-9 likely impacts the early stage of the SARS-CoV-2 viral life cycle.

Based on the results of our time-course experiments, we sought to determine whether Gal-9 affects SARS-CoV-2 viral entry. Firstly, we examined the role of Gal-9 in SARS-CoV-2 cell-surface attachment. Cells were incubated with SARS-CoV-2 at 4°C for two hours and attached SARS-CoV-2 viral particles were detected after washing the cells three times. Gal-9 induced a substantial, highly significant ($P < 0.0001$), and dose-dependent increase in cell-surface SARS-CoV-2 attachment (Figure 2A). We next

determined the capacity of Gal-9 to affect the entry of VSV-SARS-CoV-2 spike-ΔG-luciferase reporter pseudovirus (hereafter referred to as SARS-2-S) into Calu-3 cells. Positive serum (P serum), which was predetermined to possess SARS-CoV-2 neutralizing activity, potently reduced SARS-2-S infection ($P < 0.01$) but did not suppress the infection of VSV-spike G glycoprotein-luciferase reporter pseudovirus (hereafter referred to as VSV-G) (Figure 2B). Gal-9 markedly enhanced SARS-2-S infection in a dose-dependent manner in Calu-3 cells which endogenously express angiotensin-converting enzyme 2 (ACE2) and TMPRSS2 ($P < 0.01$) (Figure 2B), indicating that Gal-9 can potentiate SARS-CoV-2 attachment and entry. Unexpectedly, entry of VSV-G was also significantly enhanced by Gal-9 treatment ($P < 0.0001$), suggesting that this pro-viral activity may be generalizable to other viral taxa.

ACE2 has been identified as the critical receptor for SARS-CoV-2 binding and entry (Zamorano Cuervo and Grandvaux, 2020). To explore whether Gal-9-promoted virus entry depends on ACE2 binding, we treated cells with an anti-ACE2 antibody that competitively binds to the receptor. As expected, anti-ACE2 antibody blocked SARS-2-S but not VSV-G entry in a dose dependent manner ($P < 0.05$) (Figure 2C). Anti-ACE2 antibody also blocked Gal-9-enhanced SARS-2-S infection ($P < 0.01$) (Figure 2D), indicating that Gal-9 facilitates SARS-CoV-2 entry in an ACE2-dependent manner.

We next investigated the potential mechanisms underlying the Gal-9-mediated enhancement of SARS-CoV-2 viral entry. SARS-CoV-2 can use the endosomal cysteine proteases cathepsin B and L (CatB/L) and the serine protease TMPRSS2 to prime entry (Jackson et al., 2022). Only TMPRSS2 activity is essential for viral spread and pathogenesis in the infected host, whereas CatB/L activity is dispensable. In Calu-3

cells, which express ACE2 and TMPRSS2 (Figure 3A), SARS-CoV-2 entry was demonstrated to be primed by TMPRSS2 (Hoffmann et al., 2020). To determine if Gal-9 modulates ACE2 and TMPRSS2 surface expression to promote virus entry, we measured Calu-3 cell surface ACE2 and TMPRSS2 expression by flow cytometry. Gal-9 exhibited no effects on ACE2 and TMPRSS2 expression (Figure 3B), suggesting that Gal-9 facilitates virus entry independently of ACE2 and TMPRSS2 induction. We next investigated the direct impact of Gal-9 on the interaction between the SARS-CoV-2 spike protein and the ACE2 entry receptor, using purified spike and ACE2 proteins in an established sandwich ELISA protocol (Sama et al., 2020). Gal-9 significantly enhanced binding between ACE2 and spike ($P < 0.05$) (Figure 3C), indicating Gal-9 facilitates virus entry, and viral replication at large, by strengthening ACE2 and spike interaction.

Gal-9-mediated enhancement of SARS-CoV-2 entry is glycan-dependent

To explore the impact of Gal-9–glycan interactions on SARS-CoV-2 infection, we first determined if Gal-9-enhanced SARS-CoV-2 entry was dependent on CRD activity, relying on lactose, a competitive inhibitor of galectin carbohydrate-binding activity (Giovannone et al., 2018). Our data demonstrated that lactose treatment significantly abrogated Gal-9-mediated SARS-CoV-2 entry in a dose-dependent manner ($P < 0.001$) (Figure 4A). We then deglycosylated Calu-3 target cells using kifunensine treatment (Elbein et al., 1990). Kifunensine inhibits mannosidase I enzymatic activity within the cell, preventing hybrid and complex N-linked glycosylation of synthesized proteins. Loss of host complex N-glycans led to significant inhibition of Gal-9-enhanced SARS-CoV-2 entry ($P < 0.01$) (Figure 4B). We next investigated the effect of galectin–glycan interactions on the binding between the viral spike protein and ACE2, using PNGase F

exposure to chemically remove N-glycans from purified spike or ACE2 glycoprotein (Huang et al., 2021). PNGase F treatment of spike or ACE2 inhibited the effect of Gal-9 on binding between these two factors (P < 0.001) (Figure 4C and D), indicating that galectin–glycan interactions facilitate viral attachment. Collectively, these data demonstrate that Gal-9 promotes SARS-CoV-2 attachment and entry into host cells in a glycan-dependent manner.

Gal-9 promotes SARS-CoV-2-associated expression of pro-inflammatory cytokines

We next evaluated the temporal characteristics of Gal-9-mediated enhancement of SARS-CoV-2 replication. Our growth curves are compatible with the concept that Gal-9 facilitates SARS-CoV-2 entry, as the expression of the viral *N* gene was significantly increased within one to three hours post-infection (hpi) in Calu-3 cells (P < 0.0001), as compared to untreated controls (Figure 5A). Maximum viral yields were detected at 36 hpi with Gal-9 treatment, and 48 hpi without Gal-9 treatment, respectively. In accordance with the viral growth kinetic data, microscopy images showed that virus-mediated cytopathic effects (CPE) were much more pronounced in infected cultures treated with Gal-9 at both 36 and 72 hpi, as compared to infected, Gal-9 untreated cultures (Figure 5B). The enhancement of virus production by Gal-9 over time was also evaluated by $TCID_{50}$ in the supernatant at various time points (Figure 5C). Enhanced release of infectious virus in the presence of Gal-9 was observed as early as nine hpi (P < 0.05), again reflecting effects of Gal-9 on early stages of the viral life cycle. Collectively, these results reinforce the concept that Gal-9 promotes SARS-CoV-2 viral production through enhancement of viral entry.

The host inflammatory response drives much of the pathology, morbidity, and mortality associated with SARS-CoV-2 infection (Merad and Martin, 2020), and Gal-9 was positively correlated with pro-inflammatory mediators and disease severity in COVID-19 patients. Therefore, we sought to determine if Gal-9 promotes pro-inflammatory cytokine expression, either directly, or indirectly via enhancement of viral replication. Uninfected and/or untreated cells were also characterized as a negative control and reference. In the absence of SARS-CoV-2 infection, Gal-9 treatment alone induced *IL-6*, *IL-8*, and *TNFα* (all $P < 0.05$) gene expression in Calu-3 cells, albeit at modest levels (Figure 5D–F). In the absence of Gal-9, SARS-CoV-2 infection alone potently induced *IL-6*, *IL-8*, and *TNFα* (all $P < 0.05$) gene expression, starting at 24, 36, and 24 hpi, respectively (Figure 5D–F). In the presence of Gal-9, SARS-CoV-2 infection significantly induced *IL-6*, *IL-8*, and *TNFα* (all $P < 0.05$) gene expression, starting at 9, 12, and 9 hpi, respectively (Figure 5D–F). Gal-9 treatment of infected cultures potentiated *IL-6* ($P < 0.001$), *IL-8* ($P < 0.05$), and *TNFα* ($P < 0.05$) gene expression as compared to SARS-CoV-2 infection alone (Figure 5D–F). Moreover, Gal-9 treatment of infected cultures significantly increased *IL-6*, *IL-8*, and *TNFα* (all $P < 0.05$) gene expression as compared to Gal-9 treatment in the absence of SARS-CoV-2 infection. These observations were confirmed, in part, at the protein level by applying a bead-based immunoassay to culture supernatants. Protein measurements confirmed enhanced IL-6 ($P < 0.05$) and IL-8 secretion ($P < 0.01$) by Gal-9 in the presence of SARS-CoV-2 infection (Supplementary Figure S3A and B). TNFα and IL-17A secretion were additionally induced by Gal-9 in infected cells, although not quite achieving statistical significance (Supplementary Figure S3C and D). Considering that the effects

of Gal-9 on cytokine expression were relatively negligible in the absence of infection, our data indicate that Gal-9 and SARS-CoV-2 synergistically promote expression of pro-inflammatory cytokines in AECs. A formal quantitative analysis of synergy indeed revealed a synergistic impact of combined Gal-9 exposure and SARS-CoV-2 infection on *IL-6* and *TNFα* expression in AECs (Supplementary Figure S4).

RNA-seq analysis reveals synergistic effects of Gal-9 and SARS-CoV-2 on the host transcriptome

To understand the transcriptional impact of Gal-9-mediated enhancement of SARS-CoV-2 infection and immunopathology, we performed RNA-seq analysis on Calu-3 cells infected for 24 hours with SARS-CoV-2 in the presence or absence of 250 nM Gal-9. Uninfected and/or untreated cells were also characterized as a negative control and reference for the other three experimental conditions. Differentially-expressed gene (DEG) analysis was performed, using a false discovery rate (FDR) cutoff of 0.05. Only one protein coding gene (*RNU12*) was significantly modulated by SARS-CoV-2 infection alone (FDR = 1.89×10^{-7}) (Figure 6A). Eighty-seven genes were significantly modulated by Gal-9 treatment alone (Figure 6B), including 30 down-regulated and 57 up-regulated genes. Cells infected in the presence of Gal-9 exhibited a dramatic impact on the host transcriptome, with 1094 DEGs identified (Figure 6C), including 323 down-regulated and 771 up-regulated genes. Using ingenuity pathway analysis (IPA), we analyzed the enriched canonical pathways that overlap with the DEGs (Figure 6D). Key pro-inflammatory programs including IL-17, EIF2, IL-6, IL-8, and JAK/STAT signaling pathways were activated in infected cells in the presence of Gal-9.

A detailed interactome depicting Gal-9 and SARS-CoV-2 effects on IL-17 and IL-6 signaling pathway members are shown in Supplementary Figure S5 and S6.

DEGs were also categorized with respect to diseases and host functions, which are listed in Supplementary Figure S7A and B. The results demonstrated that inflammatory response, infectious, inflammatory, and immunological disease pathways were activated in the setting of Gal-9 treatment. Interestingly, pathways related to respiratory disease and RNA post-transcriptional modification were specifically activated in cells infected with SARS-CoV-2 in the presence of Gal-9.

We next leveraged the RNA-seq data to examine the impact of Gal-9 treatment on SARS-CoV-2 expression, achieved by aligning sequencing reads against the USA-WA1/2020 reference genome. The number of reads mapping to each region of the viral genome was calculated and interpreted to infer viral expression patterns (Figure 6E). The transcription of SARS-CoV-2 RNA exhibited an uneven pattern of expression along the genome, typically with a minimum depth in the first coding regions with open reading frames 1a and 1b, and the maximum towards the 3' end. This skewing likely reflects the relative abundance of these sequences due to the nested transcription of SARS-CoV-2 subgenomic RNAs. All viral transcript variants include the terminal 3' genome segment (Cao et al., 2021). Importantly, in accordance with our reverse transcription quantitative polymerase chain reaction (RT-qPCR) data, Gal-9 treatment increased the expression of SARS-CoV-2 RNA, resulting in a ~10-fold increase in the number of sequencing reads mapping to the USA-WA1/2020 reference (Figure 6E and F), maintaining and even amplifying the observed 3' skewing of viral transcripts.

Gal-9 enhances SARS-CoV-2 replication and increases TNFα expression in primary AECs

Finally, we sought to investigate the effect of Gal-9 treatment on SARS-CoV-2 infection and inflammatory response in primary human AECs cultured at the air–liquid interface (ALI). Recent studies have reported that human AECs represent the primary gateway for SARS-CoV-2 infection upon colonization of a new host (Djidrovski et al., 2021). Rapid viral replication in these cells lead to the release of pro-inflammatory cytokines, which causes airway damage and diminished patient survival. Thus, our ALI-cultured primary airway epithelial system is useful in modeling the *in vivo* effects of Gal-9 on SARS-CoV-2 infection *ex vivo*. We pretreated primary AECs from five healthy donors with Gal-9 and then infected them with the SARS-CoV-2 Gamma variant (Pango lineage designation P.1) for 36 hours. The Gamma variant was selected based on our observations demonstrating that the Gamma variant infects primary AECs more efficiently than the founder virus lineage (USA-WA1/2020) (data not shown). Productive infection was observed in all five donor cultures, based on expression of the SARS-CoV-2 *N* gene (Figure 7A). Validating our observations in Calu-3 cells, Gal-9 treatment significantly increased SARS-CoV-2 replication ($P < 0.05$), by up to 2.6-fold (Figure 7A). We also assessed pro-inflammatory signatures at 36 hpi by RT-qPCR. Our results showed that SARS-CoV-2 significantly induced *TNFα* expression as compared to mock control ($P < 0.05$) (Figure 7B). The mRNA levels of *IL-6* and *IL-8* were not affected by SARS-CoV-2 infection. Gal-9 treatment significantly increased *IL-6* expression level in the presence of SARS-CoV-2 ($P < 0.05$), and induction of *TNFα* was observed but failed to achieve statistical significance ($P = 0.055$) (Figure 7B). Taken together, our findings

in primary AECs validate and extend our previous observations, confirming that Gal-9 promotes SARS-CoV-2 replication and associated pro-inflammatory signaling in the airway epithelium.

Discussion

The elevation of plasma Gal-9 levels in COVID-19 cases and severe COVID-19 disease has been confirmed in multiple reports (De Biasi et al., 2020; Bozorgmehr et al., 2021). Here, we leveraged a recombinant stable-form of Gal-9 as a proxy for endogenously produced Gal-9, and investigated its impact on SARS-CoV-2 replication and host immune signaling. Our data reveal that Gal-9 enhances SARS-CoV-2 replication in AECs, including human primary ALI-cultured AECs, facilitating cellular entry in a galectin–glycan interaction-dependent manner. Our transcriptomic data show that Gal-9 accelerates and exacerbates several virus-induced pro-inflammatory programs in AECs. These observations are highly relevant to the clinical manifestations and management of COVID-19, suggesting that circulating Gal-9 has a direct impact on viral infectivity and the cytokine milieu in the airway epithelium, which constitutes the critical initial site of SARS-CoV-2 attachment and infection (Mulay et al., 2021). Collectively, our findings complement previous reports highlighting plasma Gal-9 level as a biomarker of severe COVID-19 disease, providing a novel molecular and immunologic framework linking Gal-9 activity to disease pathology (Supplementary Figure S8). Importantly, our data build on a robust literature featuring Gal-9 as a key host factor regulating viral immunopathogenesis.

We observed potent Gal-9-mediated enhancement of SARS-CoV-2 cellular entry, using both pseudoviral constructs and wildtype replication-competent viruses. Previous studies have demonstrated that Gal-9 promotes HIV entry through retaining protein disulfide isomerase on the CD4^{+} T cell surface (Bi et al., 2011). Therefore, we initially hypothesized that Gal-9 promoted SARS-CoV-2 entry by retaining or increasing viral receptor expression on the cell surface. However, our flow cytometry data revealed no impact of Gal-9 exposure on ACE2 or TMPRSS2 surface expression. These data were further validated by our transcriptomic analysis which failed to show any modulation of ACE2 or TMPRSS2 mRNA transcripts by Gal-9. Studies have found roles for Gal-9 in bridging pathogen glycans to host cell surface glycans to promote target cell attachment (Baum et al., 2014). We therefore conducted experiments to determine if this phenomenon underlies Gal-9-mediated enhancement of SARS-CoV-2 entry. Our data confirm the hypothesis that this enhancement is dependent on facilitating viral binding and attachment. This conclusion was supported by three pieces of evidence: 1) the attachment of SARS-CoV-2 virions to the cell surface is enhanced by Gal-9 through galectin–glycan interactions. 2) Gal-9 directly enhances the binding of the viral spike protein to the ACE2 receptor. 3) Gal-9 effects on SARS-CoV-2 growth kinetics reflect facilitation of an immediate-early viral life cycle stage. These findings are compatible with a provocative hypothesis reported by (Arciniegas et al., 2021) that multiple galectins act in concert through N- and O-linked glycans on the SARS-CoV-2 spike to form a galectin–glycan lattice on the virion surface, promoting viral attachment and penetration. Lujan and colleagues have recently shown that galectins including Gal-1, Gal-3, and Gal-9 can promote cell-surface binding, internalization, and cell invasion of

many sexually transmitted pathogens, including bacteria, parasites, and viruses (Lujan et al., 2022). This enhancement is mediated by bridging the pathogen surface and receptors on host tissues in a glycosylation-dependent manner (Lujan et al., 2022). Our data further revealed that the cellular entry of VSV-G, like SARS-CoV-2, is enhanced by Gal-9 exposure, suggesting that entry enhancement of multiple viral taxa could be mediated by galectin–glycan lattice interactions.

Accumulating evidence suggests that fatal COVID-19 is characterized by a profound cytokine storm (Fajgenbaum and June, 2021). The overproduction of pro-inflammatory cytokines, such as IL-6, IL-8, TNFα, and IL-1β, leads to an increased risk of vascular hyperpermeability, acute lung injury, multiorgan failure, and eventually death when the high cytokine concentrations are unabated over time (Costela-Ruiz et al., 2020). In direct relation to this phenomenon, our transcriptomic analysis revealed that Gal-9 and SARS-CoV-2 infection synergistically induced the expression of key pro-inflammatory programs in AECs, including the IL-8, IL-17, EIF2, and TNFα signaling pathways. These data were validated in part at the protein level using a bead-based immunoassay to characterize the AEC secretome. Bozorgmehr and colleagues demonstrated highly significant positive correlations of plasma Gal-9 levels with a wide range of pro-inflammatory biomarkers in COVID-19 patients. They further demonstrated that Gal-9 treatment of monocytes *in vitro* enhanced expression and production of key pro-inflammatory molecules associated with severe COVID-19 disease (Bozorgmehr et al., 2021). Gal-9 induces secretion of inflammatory cytokines in several immune cell lineages including monocyte-derived macrophages and neutrophils (Nobumoto et al.,

2009; Querol Cano et al., 2019). Our findings validate and extend these observations to SARS-CoV-2 infection of the airway epithelium.

Importantly, the combined effects of SARS-CoV-2 infection and Gal-9 exposure on pro-inflammatory signaling are much stronger than either Gal-9 or SARS-CoV-2 alone, reflecting a synergistic interaction. We observed little transcriptional perturbation by SARS-CoV-2 alone after 24 hours of infection, which is consistent with other reports that profound transcriptional changes are only evident after 48 hours (Blanco-Melo et al., 2020; Subramaniyan et al., 2021). Interestingly, the IL-17 signaling pathway was significantly activated after Gal-9 treatment in the presence or absence of SARS-CoV-2. Our data are in accordance with a previous report demonstrating induction of IL-17 signaling by Gal-9 treatment *in vivo*, in the setting of sepsis (Kadowaki et al., 2013). For MERS-CoV, SARS-CoV, and now SARS-CoV-2, disease severity has been shown to positively correlate with levels of IL-17 and other T helper 17 cell-related pro-inflammatory cytokines (Mahallawi et al., 2018; Yang et al., 2020; Hasan et al., 2021). IL-17 inhibition has been adopted as a common and successful strategy to reduce the injury associated with inflammatory autoimmune diseases (Pacha et al., 2020). Thus, inhibition or neutralization of Gal-9 would not only decrease SARS-CoV-2 replication but also attenuate IL-17 signaling and other damaging pro-inflammatory cascades.

Our study has limitations that must be considered. Firstly, we focused exclusively on the airway epithelium, and it is now established that SARS-CoV-2 is capable of infecting other cell lineages including monocytes, monocyte-derived macrophages, and microglia (Boumaza et al., 2021; Liu et al., 2021; Jeong et al., 2022). It is possible that Gal-9 does not exert similar effects on viral replication or immune signaling in other target cell

types. Secondly, our studies were all performed *in vitro* or in transplant tissue-derived primary epithelial cells *ex vivo*. As it is well-established that Gal-9 exerts conditional, pleiotropic immunomodulatory effects, the net effect of Gal-9 signaling on SARS-CoV-2 pathogenesis cannot be fully appreciated outside of an animal model with a functional immune system. Validation and extension of our observations in murine, hamster, or nonhuman primate models of SARS-CoV-2 infection will help in evaluating the clinical relevance of our reported findings. In relevance to the implementation of animal models, our study did not elucidate the principal cell or tissue sources responsible for secreting Gal-9 in the setting of SARS-CoV-2 infection. A study examining the role of Gal-9 in pulmonary fibrosis revealed that immune cells including alveolar macrophages, lymphocytes, and type II pneumocytes are the principal sources of Gal-9 production in the diseased lung (Matsumoto et al., 2013). Leveraging an animal model to identify these source compartments will be critical in developing interventions to manipulate Gal-9 signaling as a therapeutic approach.

To our knowledge, the data presented here are the first to show that Gal-9 is directly involved in enhancing SARS-CoV-2 infection and virus-induced pro-inflammatory pathology, exposing an area of vulnerability for further investigation. Our data warrant examination of Gal-9-targeting therapeutic strategies *in vivo*, designed to simultaneously inhibit viral replication and suppress deleterious immune signaling associated with COVID-19 disease. There are existing tools which may be exploited to experimentally manipulate Gal-9 *in vivo*, including administration of exogenous, recombinant stable-form Gal-9 to enhance signaling (Nishi et al., 2005). Small molecules and promising monoclonal antibodies under investigation in the clinical

oncology space (e.g. LYT-200) that antagonize Gal-9 activity may have utility in COVID-19 (Bertino et al., 2019; Filipovic et al., 2021; Yang et al., 2021). On this note, a recent exploratory clinical trial involved administration of a galectin antagonist to individuals with COVID-19 disease, revealing beneficial effects of galectin inhibition on disease outcomes (Sigamani et al., 2020). This represents a provocative and promising early step in the development of galectin-based therapeutics for SARS-CoV-2 infection in the future.

Materials and methods

Cell lines

The Calu-3 human lung adenocarcinoma epithelial cell line was obtained from ATCC (ATCCHTB-55) and cultured in Eagle's Minimum Essential Medium (EMEM). Vero E6 cells were purchased from ATCC (CRL-1586) and cultured in Dulbecco's Modified Eagle's medium (DMEM). Vero E6 cells stably expressing TMPRSS2 (Vero E6-TMPRSS2) were established and cultured in DMEM in the presence of puromycin (1μg/ml). All media were supplemented with 10% fetal bovine serum (FBS) and 1% penicillin/streptomycin. All cells had been previously tested for mycoplasma contamination and incubated at 37°C in a humidified atmosphere with 5% CO_2.

Primary AECs

Human bronchus was harvested from five explanted healthy lungs. The tissue was submerged and agitated for one minute in PBS with antibiotics and 5 mM dithiothreitol to wash and remove mucus. After three washes, the tissue was placed in DMEM with

0.1% protease and antibiotics overnight at 4ºC. The next day, the solution was agitated and the remaining tissue was removed. Cells were centrifuged at 300 g (4ºC) for five minutes, then the cell pellet was resuspended in 0.05% trypsin-EDTA and incubated for five minutes at 37ºC. The trypsinization reaction was neutralized with 10% FBS in DMEM, then cells were filtered through a cell strainer and centrifuged at 300 g (4ºC) for five minutes. The cell pellet was resuspended in DMEM with 10% FBS and 10 μl was stained with trypan-blue and counted on a hemocytometer. A total of 75000 cells were plated onto each 6 mm/0.4 mm Transwell ALI insert after treatment with FNC coating mixture (Athena Enzyme Systems, 0407). DMEM and ALI media with 10% FBS were added in equal volumes to each basal compartment and cultures were incubated at 37ºC with 5% CO_2. The next day, the media was removed and basal compartments were washed with PBS and antibiotics. ALI media was then added to each basal compartment and changed every three days until cells were ready for use at day 28.

Viruses

SARS-CoV-2 (isolate USA-WA1/2020 and isolate lineage P.1) were obtained from BEI Resources of National Institute of Allergy and Infectious Diseases (NIAID). Viruses were propagated in Vero E6-TMPRSS2 cells in DMEM with 2% FBS and 1% penicillin/streptomycin and viral stocks were stored at −80ºC. Virus titer was measured in Vero E6 cells by $TCID_{50}$ assay. All the studies involving live viruses were conducted in the Vitalant Research Institute BSL-3 under approved safety protocols.

Ethics statement

The studies involving human participants were reviewed and approved by the Human Research Protection Program, University of California, San Francisco. The patients/participants provided their written informed consent to participate in this study.

Cytotoxicity assay

The cytotoxic effect of Gal-9 on Calu-3 cells was determined using an MTT assay kit (abcam, ab211091) according to manufacturer's guidelines. In brief, Calu-3 cells cultured in 96-well cell culture plates were incubated with different concentrations of Gal-9 (0–5000 nM). After 48 hours, the media was removed and 100 μl MTT reagent (1:1 dilution in serum free DMEM medium) was added to each well and incubated for 3 h at 37ºC. Then the medium was removed, and 150 μl MTT solvent was added into each well. Quantification was performed by reading absorbance at OD = 590 nm. The data from three independent experiments was used to calculate the CC_{50} by nonlinear regression using GraphPad Prism 8.0 software.

SARS-CoV-2 infection and Gal-9 administration

Stable-form recombinant Gal-9 was used in all experiments (Nishi et al., 2005; Abdel-Mohsen et al., 2016). Calu-3 cells were seeded at 0.5×10^6 cells per well in 0.5 ml volumes using a 24-well plate, or were seeded at 1×10^5 cells per well in 0.1 ml volumes using a 96-well plate. The following day, cells were pretreated with or without Gal-9 for 6 hours. Then viral inoculum (MOI of 0.01; 500 μl/well or 100μl/well) was prepared using EMEM containing indicated concentrations of Gal-9 and added to the

wells. The inoculated plates were incubated at 37ºC with 5% CO_2. Supernatants were collected and stored at −80ºC at 24 hpi. Cells were lysed with TRizol (Thermo Fisher Scientific, 15596026) for RNA extraction or fixed with methanol:acetone (1:1) for immunofluorescence assay.

For infection of ALI-cultured primary AECs, SARS-CoV-2 (diluted in ALI-culture medium, MOI = 0.1) was added to the apical chamber of inserts (250 μl) and the basal compartment (500 μl). Then the cultures were incubated for 2 hours at 37ºC (5% CO_2) to enable virus entry. Subsequently, the cells were washed and fresh ALI medium (500 μl) was added into the basal compartment. Cells were incubated at 37ºC (5% CO_2) and harvested for analysis at 36 hpi.

Viral titer by $TCID_{50}$ assay

Viral production by infected cells was measured by quantifying $TCID_{50}$. Vero E6 cells were plated in 96-well plates at 5×10^4 cells per well. The next day, supernatants collected from Calu-3 cells were subjected to 10-fold serial dilutions (10^1 to 10^{11}) and inoculated onto Vero E6 cells. The cells were incubated at 37ºC with 5% CO_2. Three to five days post infection, each inoculated well was evaluated for presence or absence of viral CPE. $TCID_{50}$ was calculated based on the method of Reed and Muench (REED and MUENCH, 1938).

Immunofluorescence microscopy

Cells were washed with 1 × PBS, then were fixed and permeabilized with cold methanol: acetone (1:1) for 10 minutes at 4ºC. Next, cells were washed with 1 × PBS and incubated in a blocking buffer (5% goat serum, Seracare Life Sciences Inc, 55600007)

at room temperature for 30 minutes. Cells were then incubated with a primary antibody (monoclonal rabbit anti-SARS-CoV-2 N antibody, GeneTex, GTX135357) in 1 × PBS (1:1,000) overnight at 4ºC. The following day, cells were washed three times with 1 × PBS and incubated with a secondary antibody [goat anti-rabbit IgG (H+L), FITC (Thermo Fisher, 65-6111)] in 1 × PBS (1:200) for 1 hour at 37ºC. Then cells were washed three times with 1 × PBS and incubated with DAPI (300 nM, Thermo Fisher Scientific, D1306) for 5 minutes at room temperature. Images were acquired using a fluorescence microscope.

RNA-seq and IPA

RNA concentration and quality was measured using High Sensitivity RNA ScreenTape Analysis (Agilent, 5067-1500). cDNA libraries were prepared using the Illumina TruSeq Stranded total RNA library prep kit (Illumina, 20020597) and sequencing was performed on the Illumina Nextseq 550 platform generating 75 bp paired-end reads. The quality of raw sequencing reads was assessed using FastQC. DEGs were identified by GSA or ANOVA in Partek® Flow® imported into the QIAGEN IPA software application. IPA was used to identify gene ontologies, pathways, and regulatory networks to which DEGs belonged to, as well as upstream regulators (Krämer et al., 2014). Reads were also aligned to the SARS-CoV-2 isolate WA-1 and analyzed using the QIAGEN CLC Genomics Workbench.

Pseudovirus entry assay

Calu-3 cells were plated into 96-well plates. The following day, cells were pre-treated with indicated concentrations of Gal-9 for six hours. In order to block ACE2 on the cell

surface, cells were pretreated with indicated concentrations of an anti-ACE2 antibody (R&D Systems, AF933) for one hour. An unrelated anti-goat IgG antibody (R&D Systems, AB-108-C) was used as a control. Pseudovirus harboring either SARS-CoV-2 spike or VSV-G glycoprotein were diluted in EMEM containing indicated concentrations of Gal-9, and then were added to Calu-3 cells. Controls included wells with serum predetermined to possess neutralizing activity. Cells were incubated for 24 hours at 37ºC with 5% CO_2. Supernatants were then removed, cells were lysed, and luciferase activity was read using a commercial substrate (Promega, E1500).

Flow cytometry

Cells were detached with 10% EDTA containing Zombie NIR (1:300) (BioLegend, 423105) for 10 minutes at 37ºC. Then cells were washed three times with 1 × PBS and incubated with human ACE2 Alexa Fluor 488-conjugated antibody (R&D Systems, FAB9332G) or human TMPRSS2 Alexa-Fluor 594-conjugated antibody (R&D Systems, FAB107231T) or human Gal-9 PE-conjugated antibody (Biolegend, 348905) for 30 minutes at room temperature. Cells were washed three times with 1 × PBS again. Analytical flow cytometry was performed with BD LSRII flow cytometer. Data was analyzed using FlowJo.

ELISA-based assessment of SARS-CoV-2 spike binding to ACE2

Assessment of Gal-9 effects on the binding of the SARS-CoV-2 spike to human ACE2 was performed using a commercially available spike-ACE2 binding assay kit (CoviDrop SARS-CoV-2 spike–ACE2 Binding Activity/Inhibition Assay Kit, EPIGENTEK, D-1005-48) following the protocol provided by the manufacturer. Gal-9 or positive inhibitor

control was mixed with indicated amounts of recombinant human ACE2 protein, then added to an ELISA plate coated with recombinant SARS-CoV-2 spike protein and incubated at 37°C for 60 minutes. Unbound ACE2 was removed. The amount of captured ACE2, which is proportional to ACE2 binding activity, is then recognized by an ACE2 detection antibody and measured by reading the absorbance at a wavelength of 450 nm.

Image analysis

To measure the frequency of infected cells, randomly-selected areas were imaged. Each treatment had three replicates. The percentage of GFP⁺ cells was determined by dividing the number of GFP⁺ cells by the number of DAPI⁺ cells. All samples were analyzed at the same threshold values. For quantification of GFP⁺ cells, CellProfiler-3 software was used to determine the fraction of GFP⁺ cells. Briefly, we used the software pipeline CorrectIlluminationCalculate to calculate an illumination correction function for each of the two channels (DAPI, blue; GFP, green). We then used another pipeline, CorrectIlluminationApply, to load each image and correct its illumination using the pre-calculated functions. Next, we ran ColorToGray to change all slides to gray and ran IdentifyPrimaryObjects to identify the number of each channel. Finally, data were exported by using the ExportToSpreadsheet pipeline. The same threshold value was applied to the images of each area.

Quantitative analysis of synergy

The combinatorial effects of Gal-9 treatment and SARS-CoV-2 infection on pro-inflammatory cytokine expression were analyzed using the SynergyFinder web

application, implementing the Bliss Independence model. The Bliss model generates synergy scores from a response matrix (Ianevski et al., 2020).

Statistical analysis

Statistical analysis was performed using GraphPad Prism version 8 software. Data were presented as means ± SEM or median. Data were analyzed for statistical significance using an unpaired or paired Student's *t* test to compare two groups, or using a paired one-tailed Wilcoxon test. Only *P* values of 0.05 or lower were considered statistically significant (*, $P \leq 0.05$; **, $P \leq 0.01$; ***, $P \leq 0.001$; ****, $P \leq 0.0001$).

Data sharing statement

The datasets generated for this study are available on request from the corresponding author.

Conflict of interest: none declared.

Author contributions

L.D. and S.K.P. initiated the project and designed the experiments. L.D. and M.S.B. performed MTT assay. L.D. and A.G. performed and processed RNA-seq. F.D. and J.R.G. isolated and prepared ALI-cultured primary AECs. J.B. analyzed RNA-seq data. L.D., S.T.Y., and L.C.N. quantified GFP positive cells. L.D. and P.D. performed multiplex cytokine expression measurement. J.J. and G.S. performed SARS-CoV-2 stock. T.K. provided human recombinant Gal-9. L.D. and S.K.P. prepared the manuscript. Z.Y.D., J.R.G., and S.K.P. jointly supervised the work.

References

Abdel-Mohsen, M., Chavez, L., Tandon, R., et al. (2016). Human galectin-9 is a potent mediator of HIV transcription and reactivation. PLoS Pathog *12*, e1005677.

Anderson, A.C., Anderson, D.E., Bregoli, L., et al. (2007). Promotion of tissue inflammation by the immune receptor Tim-3 expressed on innate immune cells. Science *318*, 1141–1143.

Arciniegas, E., Carrillo, L.M., and Salgado, A. (2021). Potential role of galectin–glycan lattices in SARS-CoV-2 infection and pathogenesis: a hypothesis. Exploratory Research and Hypothesis in Medicine *6*, 142–145.

Bai, G., Furushima, D., Niki, T., et al. (2021). High levels of the cleaved form of galectin-9 and osteopontin in the plasma are associated with inflammatory markers that reflect the severity of COVID-19 pneumonia. Int J Mol Sci *22*, 4978.

Baum, L.G., Garner, O.B., Schaefer, K., et al. (2014). Microbe–host interactions are positively and negatively regulated by galectin–glycan interactions. Frontiers in Immunology *5*, 284.

Bertino, P., Premeaux, T.A., Fujita, T., et al. (2019). Targeting the C-terminus of galectin-9 induces mesothelioma apoptosis and M2 macrophage depletion. Oncoimmunology *8*, 1601482.

Bi, S., Hong, P.W., Lee, B., et al. (2011). Galectin-9 binding to cell surface protein disulfide isomerase regulates the redox environment to enhance T-cell migration and HIV entry. Proc. Natl Acad. Sci. USA *108*, 10650–10655.

Blanco-Melo, D., Nilsson-Payant, B.E., Liu, W.-C., et al. (2020). Imbalanced host response to SARS-CoV-2 drives development of COVID-19. Cell *181*, 1036-1045.e9.

Boumaza, A., Gay, L., Mezouar, S., et al. (2021). Monocytes and macrophages, targets of severe acute respiratory syndrome coronavirus 2: the clue for coronavirus disease 2019 immunoparalysis. J. Infect. Dis. *224*, 395–406.

Bozorgmehr, N., Mashhouri, S., Perez Rosero, E., et al. (2021). Galectin-9, a player in cytokine release syndrome and a surrogate diagnostic biomarker in SARS-CoV-2 infection. MBio *12*, e00384-21.

Cao, C., Cai, Z., Xiao, X., et al. (2021). The architecture of the SARS-CoV-2 RNA genome inside virion. Nat Commun *12*, 3917.

Chen, P.-K., Lan, J.-L., Huang, P.-H., et al. (2021). Interleukin-18 is a potential biomarker to discriminate active adult-onset still's disease from COVID-19. Frontiers in Immunology *12*, 719544.

Costela-Ruiz, V.J., Illescas-Montes, R., Puerta-Puerta, J.M., et al. (2020). SARS-CoV-2 infection: the role of cytokines in COVID-19 disease. Cytokine Growth Factor Rev *54*, 62–75.

De Biasi, S., Meschiari, M., Gibellini, L., et al. (2020). Marked T cell activation, senescence, exhaustion and skewing towards TH17 in patients with COVID-19 pneumonia. Nat Commun *11*, 3434.

Del Valle, D.M., Kim-Schulze, S., Huang, H.-H., et al. (2020). An inflammatory cytokine signature predicts COVID-19 severity and survival. Nat Med *26*, 1636–1643.

Djidrovski, I., Georgiou, M., Hughes, G.L., et al. (2021). SARS-CoV-2 infects an upper airway model derived from induced pluripotent stem cells. Stem Cells *39*, 1310–1321.

Dong, E., Du, H., and Gardner, L. (2020). An interactive web-based dashboard to track COVID-19 in real time. The Lancet Infectious Diseases *20*, 533–534.

Elbein, A.D., Tropea, J.E., Mitchell, M., et al. (1990). Kifunensine, a potent inhibitor of the glycoprotein processing mannosidase I. J Biol Chem *265*, 15599–15605.

Fajgenbaum, D.C., and June, C.H. (2021). Cytokine Storm. Reply. N Engl J Med *384*, e59.

Filipovic, A., Wainber, Z., Wang, J., et al. (2021). Phase1/2 study of an anti-galectin-9 antibody, LYT-200, in patients with metastatic solid tumors. J Immunother Cancer *9*.

Giovannone, N., Liang, J., Antonopoulos, A., et al. (2018). Galectin-9 suppresses B cell receptor signaling and is regulated by I-branching of N-glycans. Nat Commun *9*, 3287.

Han, H., Ma, Q., Li, C., et al. (2020). Profiling serum cytokines in COVID-19 patients reveals IL-6 and IL-10 are disease severity predictors. Emerg Microbes Infect *9*, 1123–1130.

Hasan, M.Z., Islam, S., Matsumoto, K., et al. (2021). SARS-CoV-2 infection initiates interleukin-17-enriched transcriptional response in different cells from multiple organs. Sci Rep *11*, 16814.

Hoffmann, M., Kleine-Weber, H., Schroeder, S., et al. (2020). SARS-CoV-2 cell entry depends on ACE2 and TMPRSS2 and is blocked by a clinically proven protease inhibitor. Cell *181*, 271-280.e8.

Hojyo, S., Uchida, M., Tanaka, K., et al. (2020). How COVID-19 induces cytokine storm with high mortality. Inflamm Regen *40*, 37.

Hu, B., Guo, H., Zhou, P., et al. (2021). Characteristics of SARS-CoV-2 and COVID-19. Nat Rev Microbiol *19*, 141–154.

Huang, H.-C., Lai, Y.-J., Liao, C.-C., et al. (2021). Targeting conserved N-glycosylation blocks SARS-CoV-2 variant infection in vitro. EBioMedicine *74*, 103712.

Ianevski, A., Giri, A.K., and Aittokallio, T. (2020). SynergyFinder 2.0: visual analytics of multi-drug combination synergies. Nucleic Acids Res *48*, W488–W493.

Iwasaki-Hozumi, H., Chagan-Yasutan, H., Ashino, Y., et al. (2021). Blood levels of galectin-9, an immuno-regulating molecule, reflect the severity for the acute and chronic infectious diseases. Biomolecules *11*, 430.

Jackson, C.B., Farzan, M., Chen, B., et al. (2022). Mechanisms of SARS-CoV-2 entry into cells. Nat Rev Mol Cell Biol *23*, 3–20.

Jeong, G.U., Lyu, J., Kim, K.-D., et al. (2022). SARS-CoV-2 infection of microglia elicits proinflammatory activation and apoptotic cell death. Microbiol Spectr *10*, e0109122.

Kadowaki, T., Morishita, A., Niki, T., et al. (2013). Galectin-9 prolongs the survival of septic mice by expanding tim-3-expressing natural killer T cells and PDCA-1$^+$ CD11c$^+$ macrophages. Crit Care *17*, R284.

Kojima, R., Ohno, T., Iikura, M., et al. (2014). Galectin-9 enhances cytokine secretion, but suppresses survival and degranulation, in human mast cell line. PLOS ONE *9*, e86106.

Krämer, A., Green, J., Pollard, J., et al. (2014). Causal analysis approaches in ingenuity pathway analysis. Bioinformatics *30*, 523–530.

Lindskog, C. (2016). The Human Protein Atlas - an important resource for basic and clinical research. Expert Rev Proteomics *13*, 627–629.

Liu, J., Li, Y., Liu, Q., et al. (2021). SARS-CoV-2 cell tropism and multiorgan infection. Cell Discov *7*, 17.

Lujan, A.L., Croci, D.O., Gambarte Tudela, J.A., et al. (2018). Glycosylation-dependent galectin–receptor interactions promote *Chlamydia trachomatis* infection. Proc. Natl Acad. Sci. USA *115*, E6000–E6009.

Lujan, A.L., Croci, D.O., Rabinovich, G.A., et al. (2022). Galectins as potential therapeutic targets in STIs in the female genital tract. Nat Rev Urol *19*, 240–252.

Machala, E.A., Avdic, S., Stern, L., et al. (2019). Restriction of human cytomegalovirus infection by galectin-9. Journal of Virology *93*, e01746-18.

Mahallawi, W.H., Khabour, O.F., Zhang, Q., et al. (2018). MERS-CoV infection in humans is associated with a pro-inflammatory Th1 and Th17 cytokine profile. Cytokine *104*, 8–13.

Matsumoto, N., Katoh, S., Yanagi, S., et al. (2013). A possible role of galectin-9 in the pulmonary fibrosis of patients with interstitial pneumonia. Lung *191*, 191–198.

Merad, M., and Martin, J.C. (2020). Pathological inflammation in patients with COVID-19: a key role for monocytes and macrophages. Nat Rev Immunol *20*, 355–362.

Miyanishi, N., Nishi, N., Abe, H., et al. (2007). Carbohydrate-recognition domains of galectin-9 are involved in intermolecular interaction with galectin-9 itself and other members of the galectin family. Glycobiology *17*, 423–432.

Moar, P., and Tandon, R. (2021). Galectin-9 as a biomarker of disease severity. Cell Immunol *361*, 104287.

Mulay, A., Konda, B., Garcia, G., et al. (2021). SARS-CoV-2 infection of primary human lung epithelium for COVID-19 modeling and drug discovery. Cell Rep *35*, 109055.

Nishi, N., Itoh, A., Fujiyama, A., et al. (2005). Development of highly stable galectins: truncation of the linker peptide confers protease-resistance on tandem-repeat type galectins. FEBS Lett *579*, 2058–2064.

Nobumoto, A., Oomizu, S., Arikawa, T., et al. (2009). Galectin-9 expands unique macrophages exhibiting plasmacytoid dendritic cell-like phenotypes that activate NK cells in tumor-bearing mice. Clin Immunol *130*, 322–330.

Pacha, O., Sallman, M.A., and Evans, S.E. (2020). COVID-19: a case for inhibiting IL-17? Nat Rev Immunol *20*, 345–346.

Patel, H., Ashton, N.J., Dobson, R.J.B., et al. (2021). Proteomic blood profiling in mild, severe and critical COVID-19 patients. Sci Rep *11*, 6357.

Premeaux, T.A., D'Antoni, M.L., Abdel-Mohsen, M., et al. (2019). Elevated cerebrospinal fluid galectin-9 is associated with central nervous system immune activation and poor cognitive performance in older HIV-infected individuals. J Neurovirol *25*, 150–161.

Querol Cano, L., Tagit, O., Dolen, Y., et al. (2019). Intracellular galectin-9 controls dendritic cell function by maintaining plasma membrane rigidity. iScience *22*, 240–255.

Reed, L.J., and Muench, H. (1938). A simple method of estimating fifty percent endpoints. American Journal of Epidemiology *27*, 493–497.

Sama, I.E., Ravera, A., Santema, B.T., et al. (2020). Circulating plasma concentrations of angiotensin-converting enzyme 2 in men and women with heart failure and effects of renin-angiotensin-aldosterone inhibitors. Eur Heart J *41*, 1810–1817.

Sanz, M., Madrid-Elena, N., Serrano-Villar, S., et al. (2021). Effect of the use of galectin-9 and blockade of the TIM-3 receptor in the latent cellular reservoir of HIV-1. J Virol *95*, e02214-20.

Sehrawat, S., Reddy, P.B.J., Rajasagi, N., et al. (2010). Galectin-9/TIM-3 interaction regulates virus-specific primary and memory CD8^{+} T Cell response. PLOS Pathogens *6*, e1000882.

Shahbaz, S., Dunsmore, G., Koleva, P., et al. (2020). Galectin-9 and VISTA expression define terminally exhausted T cells in HIV-1 infection. J Immunol *204*, 2474–2491.

Sigamani, A., Shetty, S., Madhavi, et al. (2020). Galectin antagonist use in mild cases of SARS-CoV-2; pilot feasibility randomised, open label, controlled trial. medRxiv, https://doi.org/10.1101/2020.12.03.20238840

Subramaniyan, B., Larabee, J.L., Bodas, M., et al. (2021). Characterization of the SARS-CoV-2 host response in primary human airway epithelial cells from aged individuals. Viruses *13*, 1603.

Yang, R., Sun, L., Li, C.-F., et al. (2021). Galectin-9 interacts with PD-1 and TIM-3 to regulate T cell death and is a target for cancer immunotherapy. Nat Commun *12*, 832.

Yang, X., Yu, Y., Xu, J., et al. (2020). Clinical course and outcomes of critically ill patients with SARS-CoV-2 pneumonia in Wuhan, China: a single-centered, retrospective, observational study. Lancet Respir Med *8*, 475–481.

Zamorano Cuervo, N., and Grandvaux, N. (2020). ACE2: evidence of role as entry receptor for SARS-CoV-2 and implications in comorbidities. ELife *9*, e61390.

Zhuo, Y., Zhang, Y.-F., Wu, H.-J., et al. (2017). Interaction between Galectin-9/TIM-3 pathway and follicular helper CD4^{+} T cells contributes to viral persistence in chronic hepatitis C. Biomed Pharmacother *94*, 386–393.
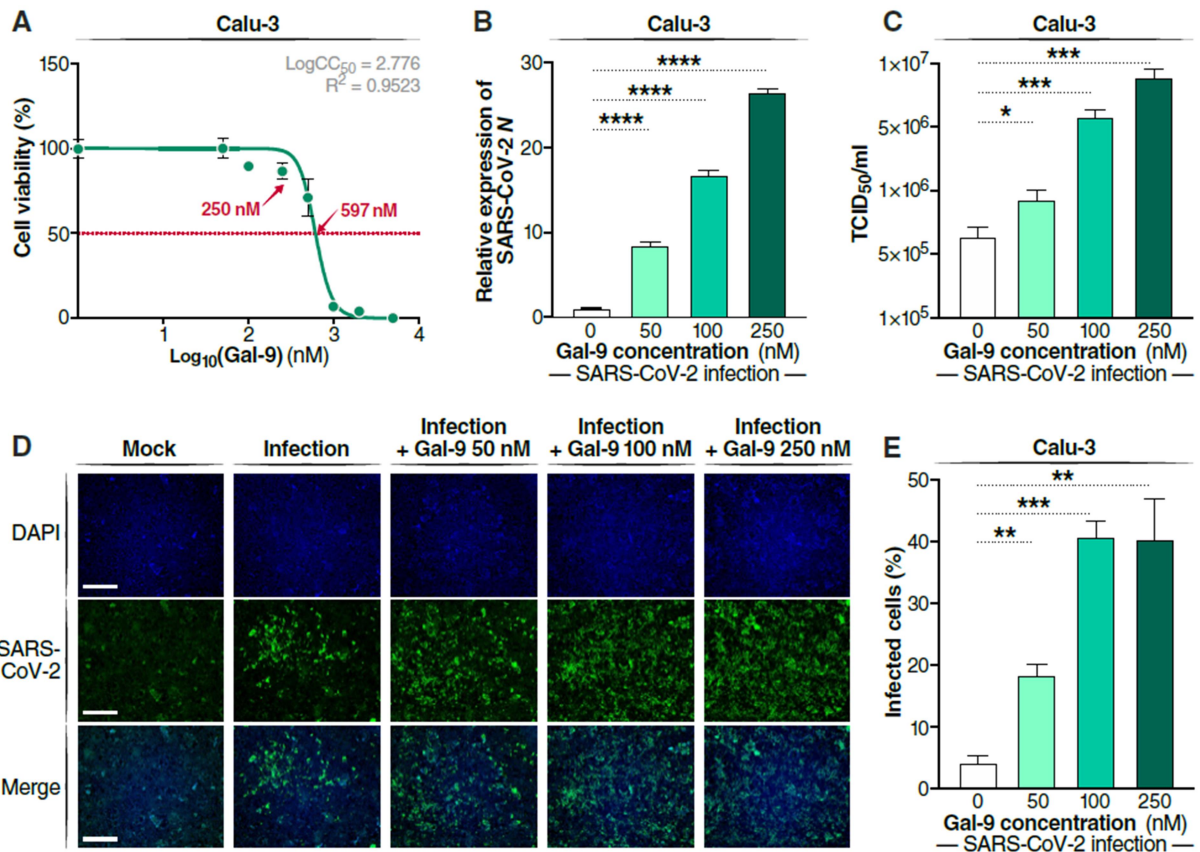
Figure 1 Gal-9 increases virus production in SARS-CoV-2-infected Calu-3 cells. (**A**) Cellular toxicity was examined in Calu-3 cells using an MTT assay and was expressed as relative cell viability as compared to Gal-9-untreated control (set at 100%). The $LogCC_{50}$ value for Gal-9 is displayed. The red arrows represent 250 nM and the CC_{50} value (597 nM) of Gal-9, respectively. (**B**) The effect of Gal-9 on viral *N* gene expression in Calu-3 cells was measured by RT-qPCR. Cells were pretreated with Gal-9 at the indicated concentrations for six hours, followed by infection with SARS-CoV-2 (MOI = 0.01) for 24 hours in the presence of Gal-9. Cells were then collected for RNA isolation

and RT-qPCR targeting the *N* gene. (**C**) Infectious virus release in the supernatant of SARS-CoV-2-infected Calu-3 cells treated with varying doses of Gal-9 as described in **B** were measured using $TCID_{50}$. (**D**) Calu-3 cells were pretreated with Gal-9 at the indicated concentrations for six hours, followed by infection with SARS-CoV-2 (MOI = 0.01) for 24 hours in the presence of Gal-9. Images presented the immunofluorescence staining of these cells with DAPI (blue) or anti-N antibody (green). Scale bar, 500 μm. (**E**) Quantification of the percentage of SARS-CoV-2 infected cells in total Calu-3 cells (shown in panel **D**). Data are representative of the results of three independent experiments (mean ± SEM). Statistical significance was analyzed by *t* test. *, $P \leq 0.05$; **, $P \leq 0.01$; ***, $P \leq 0.001$; ****, $P \leq 0.0001$.
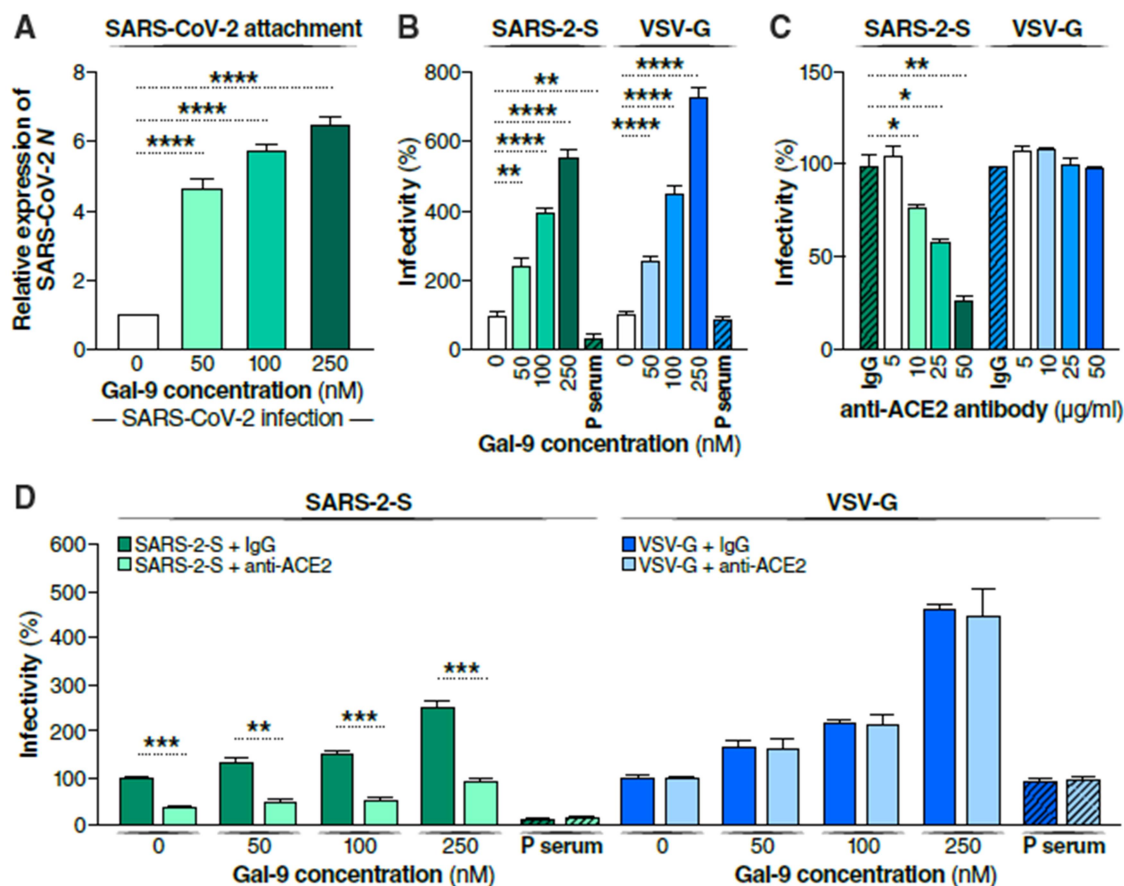
Figure 2 Gal-9 facilitates the cellular attachment and entry of SARS-CoV-2. (**A**) Attached SARS-CoV-2 virions on the cell surface were detected by RT-qPCR. Calu-3 cells were pretreated with Gal-9 for one hour, then cells were incubated with SARS-CoV-2 (MOI = 0.01) in solutions with or without Gal-9 at the indicated concentrations at 4ºC for two hours. Cells were washed three times with PBS and harvested for RNA isolation and RT-qPCR measurement of SARS-CoV-2 *N* gene expression. (**B**) Relative infectivity of SARS-2-S pseudotyped virus and VSV-G pseudotyped virus in Calu-3 cells

treated with Gal-9 at the indicated concentrations. Calu-3 cells were exposed to Gal-9 for six hours and then infected with SARS-2-S pseudotyped virus or VSV-G pseudotyped virus in solutions containing Gal-9 at the indicated concentrations. Pseudotyped viral entry was analyzed by luciferase activity 24 hpi. Positive serum predetermined to possess anti-SARS-CoV-2 neutralizing activity was used as a negative control. Luciferase signals obtained in the absence of Gal-9 were used for normalization. (**C**) Relative infectivity of SARS-2-S pseudotyped virus and VSV-G pseudotyped virus in Calu-3 cells treated with anti-ACE2 antibody at the indicated concentrations. (**D**) The effect of anti-ACE2 antibody on Gal-9-enhanced cell entry of SARS-2-S was evaluated by measuring luciferase activity. Calu-3 cells were pretreated with Gal-9 for six hours and then pre-incubated with anti-ACE2 antibody (25 µg/ml) or control antibody (25 µg/ml) for one hour, and cells were inoculated with SARS-2-S pseudotyped or VSV-G pseudotyped virus in a solution containing Gal-9 at the indicated concentrations. At 24 hpi, pseudotyped viral entry was analyzed by luciferase activity. Luciferase signals obtained in the absence of both Gal-9 and anti-ACE2 antibody were used for normalization. Data are representative of the results of three independent experiments (mean ± SEM). Statistical significance was analyzed by *t* test. *, $P \leq 0.05$; **, $P \leq 0.01$; ***, $P \leq 0.001$; ****, $P \leq 0.0001$.
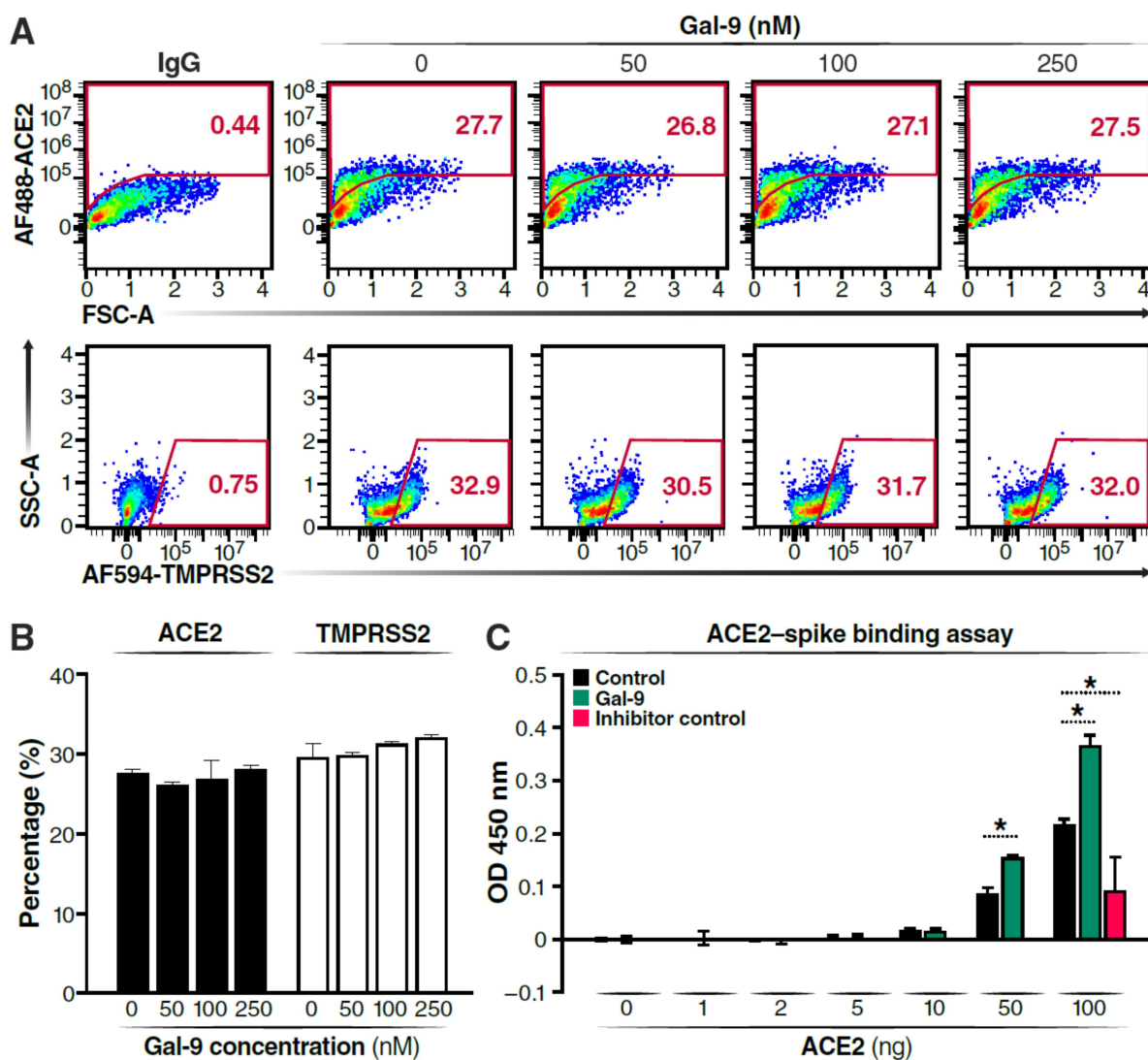
**Figure 3** Gal-9 enhances the binding of SARS-CoV-2 spike to ACE2 without affecting ACE2 and TMPRSS2 cell surface expression. (**A**) Representative flow cytometry plot describing the protein levels of ACE2 and TMPRSS2 on the surface of Calu-3 cells treated with Gal-9. Calu-3 cells were treated with Gal-9 at the indicated concentrations for 24 hours. Cells were then washed and detached before antibody staining for flow

cytometry. (**B**) Percentages of cells expressing ACE2 or TMPRSS2 at the cell surface, measured using flow cytometry. Data represent the results of three independent experiments (mean ± SEM). (**C**) The dose-response of SARS-CoV-2 spike–ACE2 binding activity measured by reading the absorbance at the wavelength of 450 nm. Data are representative of the results of three independent experiments (mean ± SEM). Statistical significance was analyzed by *t* test. *, $P \leq 0.05$; **, $P \leq 0.01$; ***, $P \leq 0.001$; ****, $P \leq 0.0001$.
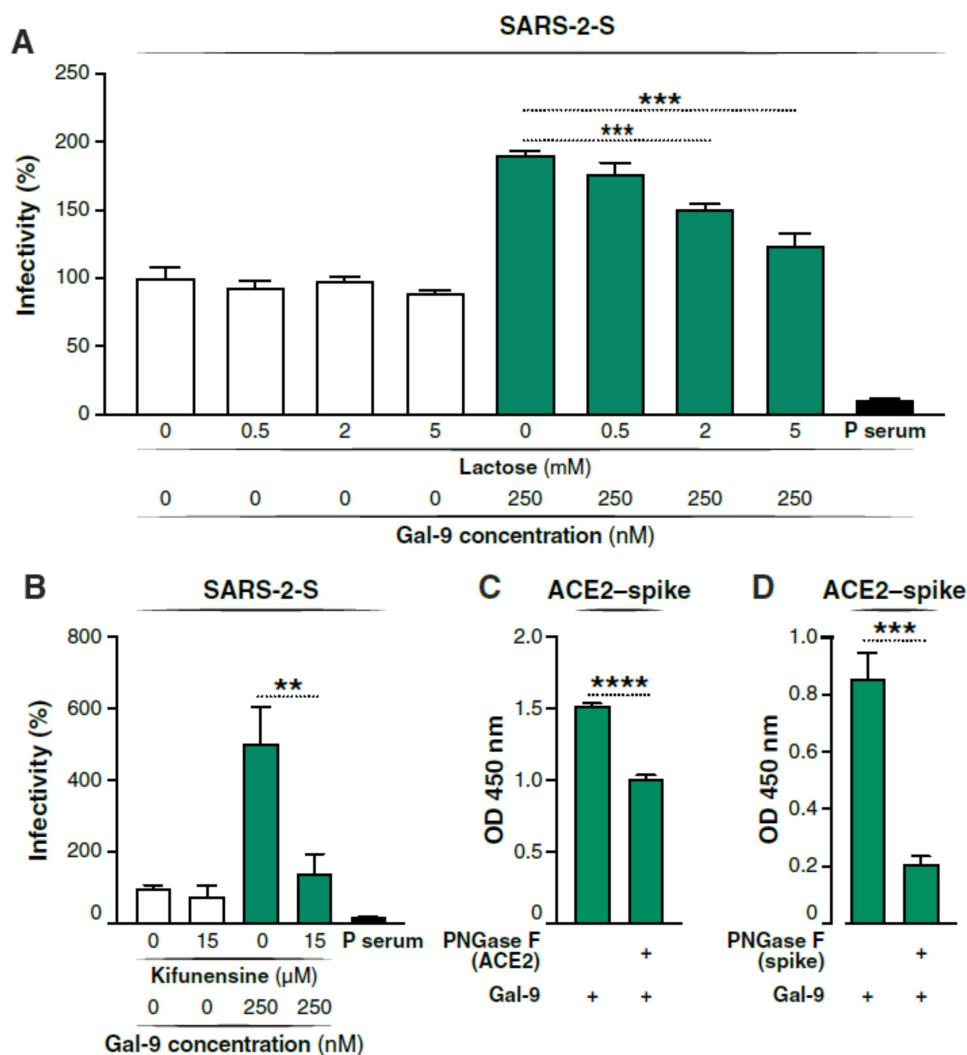
Figure 4 Gal-9 mediated enhancement of SARS-CoV-2 entry is glycan dependent. (**A**) The effect of lactose on Gal-9-enhanced SARS-CoV-2 infection was evaluated by measuring luciferase activity. Calu-3 cells were pre-treated with Gal-9 and lactose at the indicated concentrations for six hours. Cells were then inoculated with SARS-2-S pseudotyped virus in a solution containing Gal-9 and lactose at indicated concentrations. Pseudotyped viral entry was analyzed by luciferase activity at 24 hpi. Luciferase signals

obtained in the absence of Gal-9 and lactose were used for normalization. (**B**) The effect of kifunensine on Gal-9-enhanced SARS-CoV-2 entry was detected by measuring luciferase activity. Calu-3 cells were pre-incubated with kifunensine for 24 hours. Cells were then treated with Gal-9 and kifunensine for six hours. Cells were then inoculated with SARS-2-S pseudotyped virus in a solution containing Gal-9 and kifunensine at the indicated concentrations. Pseudotyped viral entry was analyzed by luciferase activity at 24 hpi. P Serum predetermined to possess anti-SARS-CoV-2 neutralizing activity was used as a positive control. Luciferase signals obtained in the absence of Gal-9 and kifunensine were used for normalization. (**C** and **D**) The effect of PNGase F on Gal-9-enhanced binding between spike and ACE2 was measured by reading the absorbance at 450 nm wavelength. ACE2 and spike-coated plates were pre-incubated with PNGase F at 37ºC for 16 hours. Signals obtained in the absence of Gal-9 and PNGase F were used for normalization. Data are representative of the results of three independent experiments (mean ± SEM). Statistical significance was analyzed by *t* test. *, $P \leq 0.05$; **, $P \leq 0.01$; ***, $P \leq 0.001$; ****, $P \leq 0.0001$.
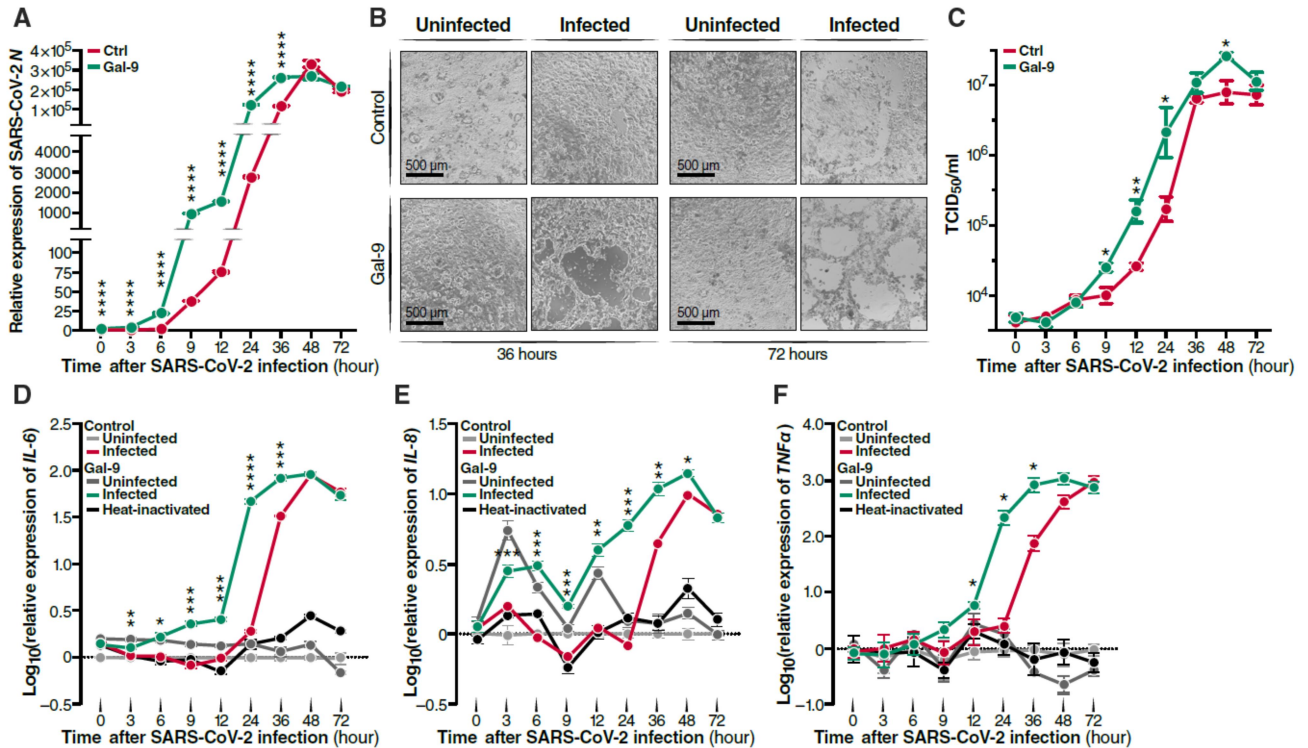
Figure 5 Gal-9 accelerates and increases SARS-CoV-2-mediated inflammatory response. (**A**) SARS-CoV-2 growth curves in Calu-3 cells pre-treated with or without Gal-9 (250 nM) for six hours and then infected with SARS-CoV-2 (MOI = 0.01) in the presence or absence of Gal-9. Cells were collected at the indicated times for RNA isolation and RT-qPCR targeting *N* gene. (**B**) Calu-3 cells from panel **A** were observed for development of CPE by bright-field microscopy at 36 hpi and 72 hpi. Scale bar, 500 μM. (**C**) Viral titer ($TCID_{50}$/ml) of supernatant collected at the indicated time points in Calu-3 cells treated as described in **A**. (**D**–**F**) mRNA levels of pro-inflammatory cytokines *IL-6* (**D**), *IL-8* (**E**), and *TNFα* (**F**) were detected by RT-qPCR at the indicated

time points. 'Heat-inactivated' indicates cells infected with heat-inactivated (non-infectious) SARS-CoV-2 (negative control). Data are representative of the results of three independent experiments (mean ± SEM). Statistical significance was analyzed by *t* test. *, $P \leq 0.05$; **, $P \leq 0.01$; ***, $P \leq 0.001$; ****, $P \leq 0.0001$.
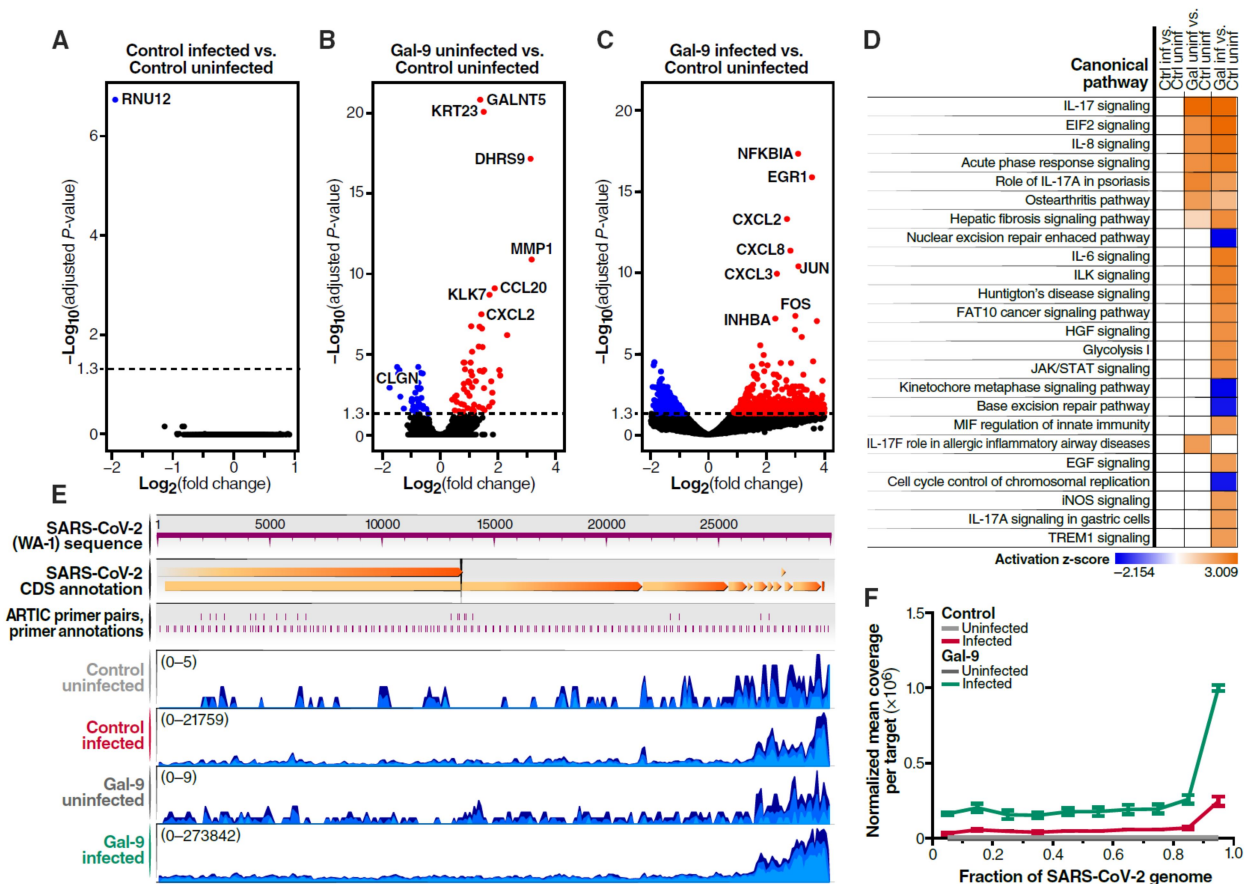
Figure 6 Impact of Gal-9 treatment on the transcriptome of SARS-CoV-2-infected Calu-3 cells. (**A**–**C**) Volcano plots showing the proportion of DEGs in the setting of SARS-CoV-2 infection (control infected vs. control uninfected) (**A**), Gal-9 treatment (Gal-9 uninfected vs. control uninfected) (**B**), and SARS-CoV-2 infection in the presence of Gal-9 (Gal-9 infected vs. control uninfected) (**C**). DEGs (FDR < 0.05) with Log2(fold change) > 0 are indicated in red. DEGs (FDR < 0.05) with Log2(fold change) < 0 are indicated in blue. Non-significant DEGs are indicated in black. (**D**) Top enriched canonical pathways identified using IPA. The orange and blue-colored bars in the bar

chart indicate predicted pathway activation or inhibition, respectively, based on z-score. Ctrl, control; Gal, Gal-9; inf, infected with SARS-CoV-2 (MOI = 0.01); uninf, uninfected with SARS-CoV-2. (**E**) Sample coverage tracks from the QIAGEN genome browser depicting SARS-CoV-2 assembly. Sample coverage tracks were obtained by mapping raw sequencing reads to the USA-WA1/2020 reference genome. Mapped read counts of control uninfected, control infected, Gal-9 uninfected, and Gal-9 infected are 0–5, 0–21759, 0–9, and 0–273842, respectively. (**F**) Normalized mean coverage per targeted region of the SARS-CoV-2 genome. The X axis represents the relative target region positions of the SARS-CoV-2 genome. Data were normalized to the total read depth for each sample.
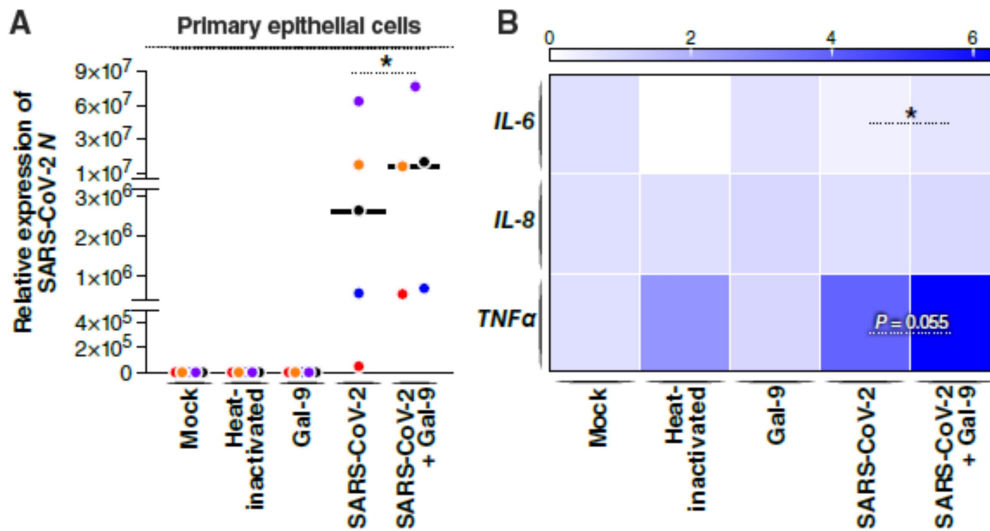
Figure 7 Gal-9 enhances SARS-CoV-2 replication and virus-induced inflammatory response in human primary AECs. (**A**) The primary epithelial cells cultured at the ALI were treated with Gal-9 at a concentration of 250 nM for six hours. Following this pre-incubation, the cells were infected with SARS-CoV-2 lineage P.1 at the MOI of 0.1, or with heat-inactivated virus, or were left uninfected (mock control). The infection was carried out by exposing the cells to a solution of Gal-9 (250 nM) in both the apical chamber (250 µl) and the basal compartment (500 µl) of the inserts for a period of two hours. Cells were washed and supplemented with fresh media alone or fresh media containing Gal-9 (250 nM). At 36 hpi, cells were collected for RNA isolation and RT-qPCR analysis of the SARS-CoV-2 *N* gene. Each color represents data from one donor. (**B**) The mRNA levels of pro-inflammatory cytokines *IL-6*, *IL-8*, and *TNFα* were

measured by RT-qPCR in primary epithelial cells treated as described in **A** in five different donors. Data represent duplicate experiments for each donor (median). Statistical significance was analyzed by paired one-tailed Wilcoxon tests. *, $P \leq 0.05$; **, $P \leq 0.01$; ***, $P \leq 0.001$; ****, $P \leq 0.0001$.